Engineering Structures 306 (2024) 117739

Contents lists available at ScienceDirect

Engineering Structures

journal homepage: www.elsevier.com/locate/engstruct

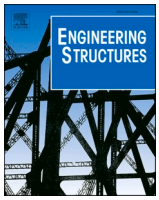

Structural design of reinforced earthcrete (ReC) beams

M. Franciosi [a], V. Savino [a], L. Lanzoni [b,*], A.M. Tarantino [b], M. Viviani [a]

[a] HEIG-VD/HES-SO - Haute Ecole d'Ingénierie et de Gestion du Canton de Vaud, Route de Cheseaux 1, CH-1401 Yverdon, Switzerland
[b] Department of Engineering "Enzo Ferrari", University of Modena and Reggio Emilia, 41125 Modena, Italy

ARTICLE INFO

Keywords:
Flexural behavior
Earthen materials
Eco-building construction
Four point testing
Adherence strength

ABSTRACT

This paper presents the results of an extensive experimental campaign aimed at evaluating the feasibility of using steel-reinforced earthen materials for load-bearing structural applications, with a focus on a new category termed "shot-earth". Addressing excavated soil, a major source of construction waste, shot-earth demonstrates remarkable properties, such as notable green strength and reduced water sensitivity. The experimental program includes four-point bending tests on steel-reinforced shot-earth beams, along with pull-out tests to assess the adherence between ribbed steel bars and shot-earth. A flexural design approach, traditionally suited for reinforced concrete, is presented and validated to establish a reliable model for reinforced shot-earth elements in bending state. These findings suggest that leveraging existing models for reinforced concrete can overcome some traditional challenges associated with earth-based constructions, promoting them as a viable and ecological alternative to conventional construction materials.

1. Introduction

Earthen construction has stood the test of time, serving as a fundamental resource for building projects around the world for centuries. Its enduring appeal among the scientific community stems from its unique attributes that combine sustainability with utility [1]. Three notable advantages of utilizing earth building materials are: (i) Their potential to reduce CO2 emissions, given that even when stabilized, earthen constructions contain a lower amount of cement compared to other materials [2,3]. (ii) The cost-saving benefits arising from the direct use of excavated soil in the field. (iii) The natural aesthetic value they confer [1,4]. Currently, the predominant methods of earth-based construction — suitable for the erection of single or two-story civil buildings — involve the use of adobe, cob, and rammed-earth techniques [1,4].

Recently, a soil-based construction material known as "shot-earth" (hereafter referred to as "SE") has been introduced to the global scientific community, with studies undertaken to analyze its mechanical, thermal, and hygrothermal properties [5–10]. SE represents a new category of sustainable construction materials composed of excavated soil, aggregates, and a small amount of stabilizer, if dictated by performance requirements. To minimize the depletion of natural resources, the utilization of recycled aggregates is preferred in the manufacturing of SE. Stabilization can be achieved not only through the addition of cement but also by incorporating agents with a lower carbon footprint, such as lime, hydraulic lime, and plaster. The mixture of raw materials undergoes a high-speed projection process allowing for the spraying of SE into formworks, which ensures a high degree of compaction. This fabrication process, rooted in shotcrete technology, imbues SE with green strength. Following a standard 28-day curing period, SE attains a compressive strength exceeding 9 MPa [5].

The interest in SE is steadily growing, driven by compelling research that not only showcases its potential applications but also elucidates its limitations, offering clear guidelines to architects, engineers, contractors, and building owners.

Often, classic earthen materials still face significant challenges in being accepted as structural materials [11] due to prejudices related to: (i) low compressive strength, albeit it can exceed 5 MPa when stabilized with cement [12,13]; (ii) water sensitivity; (iii) high maintenance requirements; and (iv) the absence of predictive models to accurately calculate and detail structural members. These prejudices can be overcome through innovation and research. To equip structural designers with the tools necessary to build safely with SE, numerous research studies have been undertaken. This paper presents the study and validation of a mechanical model devised to forecast the flexural response of reinforced SE beams. This model builds upon those established for concrete structures. Capitalizing on the existent knowledge of RC, the model modifies and tailors it to accommodate the distinct characteristics of earthen materials reinforced with steel. This approach paves the way for designs that are both reliable and sustainable in the construction of

* Corresponding author.
E-mail address: luca.lanzoni@unimo.it (L. Lanzoni).

https://doi.org/10.1016/j.engstruct.2024.117739
Received 24 September 2023; Received in revised form 22 January 2024; Accepted 20 February 2024
Available online 6 March 2024

Nomenclature

SE	Shot-earth.
RC	Reinforced concrete.
SE772	SE mix design composed by 7 parts of soil, 7 parts of aggregates and 2 parts of cement by weight.
SE772 *	SE mix design with the same proportion of SE772 but with the use of a different streak of earth.
B_SE772	SE772 beams for the four-point bending test.
P_SE772 * _l_ ø	SE772 * prisms for the pull-out test with an embedding length "l" and a rebar diameter "ø".
SE772 * _C-28	Cubic samples for SE772 * characterization in terms of C-28 and BD.
C-28	28-days compressive strength.
BD	Bulk density.
EM	Elastic modulus.
EM_{SE}	SE Elastic modulus.
EM_{SE772}	SE772 Elastic modulus.
χ	Curvature.
M_a	Bending moment for a defined cross section corresponding to a specific value of χ.
M_0	Midspan moment due to the self-weight load of the reinforced B_SE772.
J	Inertia modulus of the cross section.
J_{om}	Inertia modulus of the homogenized cross section.
δ	Midspan displacement.
P	Total load applied during the four-point bending test.
P_1	Load applied by the first servo-hydraulic actuator in the four-point bending test.
P_2	Load applied by the second servo-hydraulic actuator in the four-point bending test.
P_{min}	Minimum load applied in phase S1.
P_{max}	Maximum load applied in phase S1.
P_u	Maximum load recorded during the four-point bending test.
M_u	Maximum bending moment recorded during the four-point bending test.
$\delta(M_u)$	Midspan displacement at M_u.
$M^R(z_1)$	Bending moment for the real frame B_SE772 in the variable z_1.
$M^f(z_1)$	Bending moment for the fictional frame B_SE772 in the variable z_1.
$M^R(z_2)$	Bending moment for the real frame B_SE772 in the variable z_2.
$M^f(z_2)$	Bending moment for the fictional frame B_SE772 in the variable z_2.
S1	First loading step in the four-point bending test configuration.
S2	Second loading step in the four-point bending test configuration.
δ_{int}	Intrados displacement measured by horizontal LVDTs glued on the bottom fiber during the S1.
δ_{ext}	Extrados displacement measured by horizontal LVDTs glued on the top fiber during the S1.
LVDT	Linear Variable Displacement Transducer.
l_{cr}	LVDT characteristic length.
h	B_SE772 cross section height.
L	B_SE772 span length.
τ	Bond stress.
τ_{max}	Average bond stress from experimental results.
$\tau_{max,CEB}$	Average bond stress from concrete predicted model.
s	Slip.
$F_{P\_SE772^*,max}$	Pull out force.
ø	Rebar diameter.
l	Embedded length.
f_{cm}	Mean cylinder compressive strength.
C_{min}	Minimum cover thickness.
C_{max}	Maximum cover thickness.
K_{tr}	Efficiency of the confinement coefficient.

earthen structures.

This paper presents experimental results to validate the proposed model. Within the structural investigation, three reinforced SE beams (labeled hereafter "B_SE772") are analyzed.

The bond between concrete and steel rebars is a pivotal factor in determining the flexural performance of reinforced concrete members [14]. Accordingly, to scrutinize the bond behavior between SE772 and steel bars, six pull-out tests were conducted. Subsequently, a critical comparison was undertaken involving the bond stress–slip relationship delineated in the CEB-FIP model code 90 [15] and the CEB-FIP model code 2010 [16]. The bond behavior can also be influenced by the coefficient of thermal expansion between materials. As the constituent materials used in the production of shot-earth are the same as those employed in general earth-based materials, the conclusions drawn for rammed Earth and Compressed Stabilized Earth Block materials can be extrapolated to shot-earth, specifically the identical coefficient of thermal expansion between steel and shot-earth, as stated in [17,18].

2. Materials and methods

2.1. Materials and mixture proportions

SE represents a novel class of sustainable construction materials composed of excavated soil, aggregate (sized 0–8), stabilizing agents, and water. In the experiments, the mix proportion designated as SE772 (mix proportion by mass: 7 parts of soil, 7 parts of aggregates, and 2 parts of cement) was employed for four-point loading bending test of the reinforced SE beams. The same mix proportion was exploited for the pull-out tests. However, it is worth noting that two distinct types of soil were used for each test. As a result, the mix used in the pull-out tests will be subsequently referred to as SE772 * . The purpose of the pull-out tests is to assess, for a generic SE772 recipe, whether the assumption of perfect adhesion proves to be valid, assuming that minor variations in the composition of the earth do not affect the bonding behavior. In order to characterize the soils, a particle size analysis was conducted to assess its granulometric distribution according to the EN 933–1 standard [19], see Fig. 1. Additionally, the USCS classification was established [20], leading to the conclusion that SE772 can be grouped into CL-ML, while SE772 * falls into the CL category. The extraction of both soils occurred at a depth greater than 60 cm to avoid the presence of organic material.

The water content in the mix stands at 8.66% of the dry mixture's mass, as detailed in [6]. The application of SE involves a high-speed (300 km/h) dry projection process using a specially designed machine. This rapid projection technique endows SE with a notable density (approximately 2100 kg/m^3) and significant green strength immediately post-placement, as it is capable of maintaining its shape inside the formwork without visible deformations and without cracking before reaching its maximum strength. For constructing load-bearing structures, such as beams, SE is reinforced using steel rods compliant with the Swiss standard type B500B. This reinforcement method aligns with the recommendations for concrete beam reinforcement. The same steel rods were also incorporated in the pull-out test specimens.

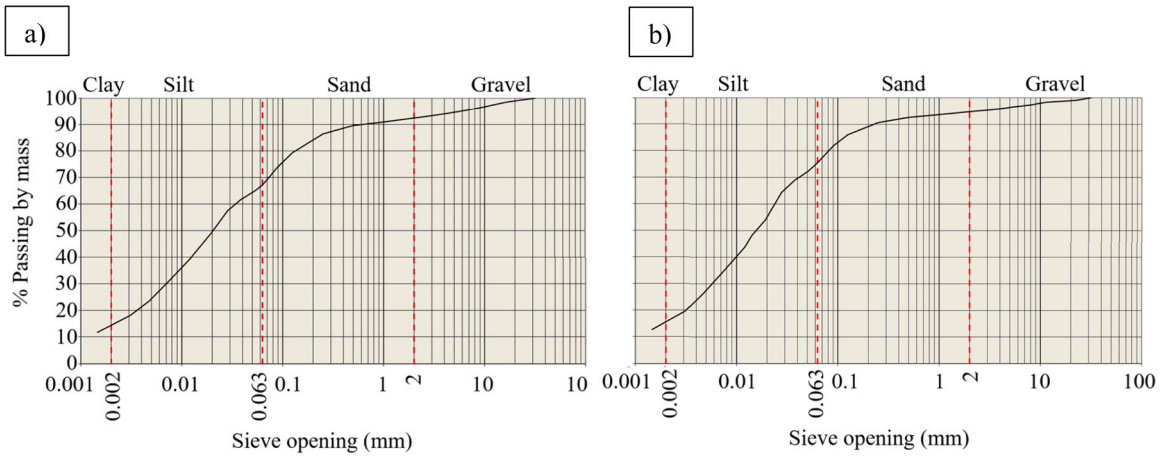

Fig. 1. Granulometric analysis of: a) SE772 soil, b) SE772 *soil.

2.2. Fabrication and curing of test specimens

To perform the four-point loading bending tests, three prismatic samples of length 4000 mm and size 300 × 400 mm^2 were constructed. The geometric features and the layout of the longitudinal and shear steel reinforcements are sketched in Fig. 2.

The mix design used for the SE beams aligns with the methodology employed in [5], ensuring consistent mechanical properties across the samples. Fig. 3 captures the step of projecting SE into the formworks. It is important to highlight that a specific spray angle is necessary to prevent aggregate bounding and to achieve optimal compaction.

Given that perfect adherence between SE and steel rebars cannot be taken for granted, several pull-out tests were conducted. To facilitate this, prismatic SE samples measuring 150 × 150 x 300 mm^3 (hereafter referred to as "P_SE772 *_l_ ø") were crafted. In the P_SE772 * _l_ ø label, l denotes the embedded length, while ø represents the steel rebar diameter (expressed in mm). A different geometry can alter the results in terms of the bond stress-slip relationship, as it can also influence the failure mechanism. The shear bond stress at failure exhibits a decreasing trend with an increase in specimen size. Experimental findings documented in [21] suggest that larger specimens, featuring correspondingly larger bars, are prone to failure in a more brittle, splitting mode. Conversely, smaller bars tend to undergo a less brittle or more plastic shear pullout mode upon failure. This shift in failure modes based on specimen size aligns with the physical implications of the size effect law [22]. For the purpose of the test, it was chosen to have an upper concrete cover greater than 5ø, ensuring a good confinement condition according to [16]. This configuration also aligns to various tests documented in the Literature [23,24]. The bar diameter for all pull-out tests is set at 12 mm, matching the specifications employed in the bending tests conducted on the beams.

Within each sample, a single steel rebar was embedded, as depicted in Fig. 4. These specimens, with varied embedded lengths (10ø and 15ø), were grouped and tested in sets of three for each specified length.

To evaluate the bulk density (subsequently termed "BD") and the 28-day compressive strength (referred to as "C-28") of SE772 * , an additional four cubical specimens with dimensions of 150 × 150 x 150 mm^3 were produced.

All specimens were cast on a single day at a construction site in Moudon, Western Switzerland. After a curing period of 7 days under summertime external conditions, the specimens were transported to the laboratory at Haute Ecole d'Ingénierie et de Gestion du Canton de Vaud (HEIG-VD) to complete the curing (28 days) at T = 23 ± 3 °C and RH = 50 ± 5%. The curing process does not involve immersion in water, as

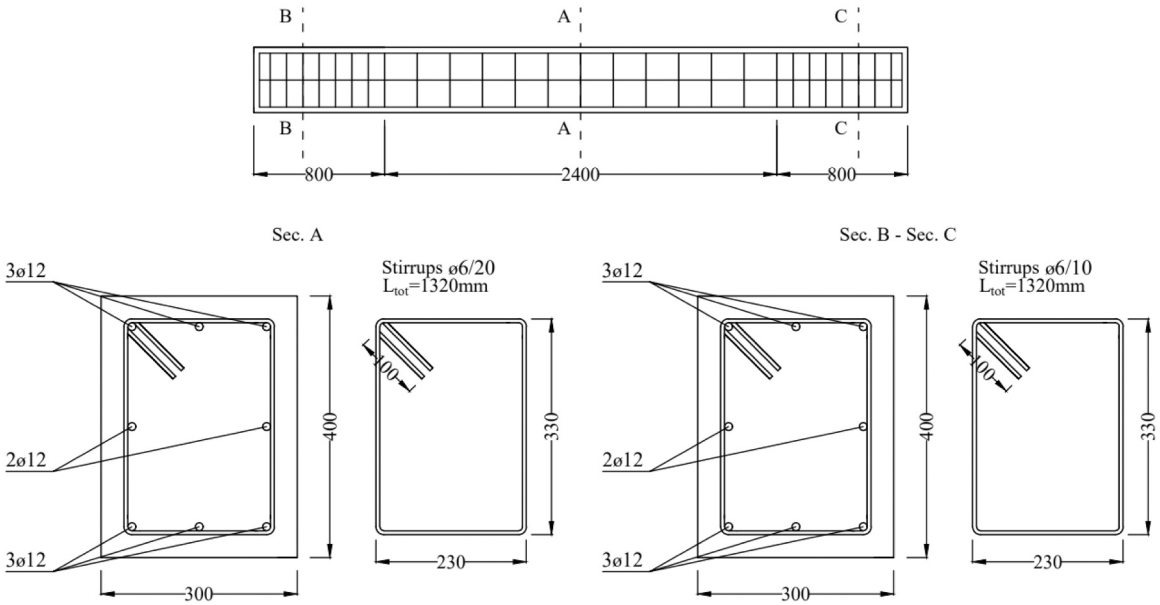

Fig. 2. B_SE772: layout of the longitudinal and shear steel reinforcements.

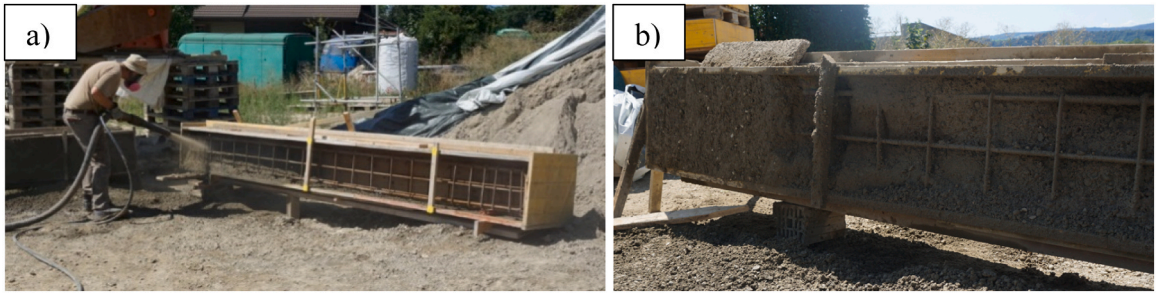

Fig. 3. a) Fabrication of B_SE772, b) B_SE772 realized portion during the projection process.

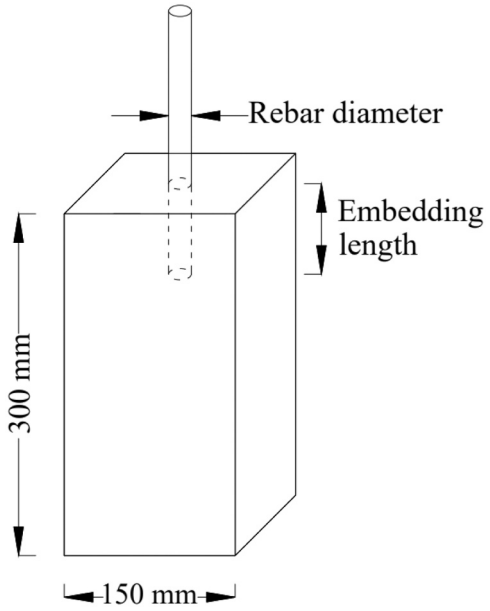

Fig. 4. SE772 sample used to perform the pull-out test.

this could result in strength losses due to the presence of soil in the mix proportion, making it susceptible to water.

An overview of the executed tests and their corresponding standards can be found in Table 1.

2.3. Compressive test

To ascertain the C-28 for the SE772 * mixture, uniaxial unconfined compressive tests were executed in line with the European standard used for concrete materials [26]. These compressive assessments were carried out utilizing a 5000 kN Perrier testing apparatus. The procedure entailed an initial preload of 15 kN, followed by a loading rate of 0.3 MPa/s, consistent with the standards.

Table 1
Experimental tests carried out on specimens.

Specimens	Label	Test	Regulation
SE772 * Prism $0.15 \times 0.15 \times 0.3$ m^3	P_SE772 * _ $l^{(a)}$_ $\phi^{(b)}$_i	Pull-out test	[14,25]
SE772 * Cubes $0.15 \times 0.15 \times 0.15$ m^3	SE772 * _C-28_i	Compressive test	[26]
SE772 Beams $0.3 \times 0.4 \times 4$ m^3	B_SE772	Four-point loading bending test	[27–30]

(a): Embedding length (mm)
(b): Steel rebar diameter (mm)
* Different streak of earth used
i: Sample number

2.4. Pull-out test

The bond between steel rebars and SE772 * was assessed using pull-out tests. Each test was conducted by applying a consistent slipping speed of 0.03 mm/s, as cited in [25,31]. The total displacement of the rebar in relation to the SE772 * support was gauged using a specific LVDT sensor setup, as illustrated in Fig. 5. Both the LVDT displacement readings and the pull-out force were captured at a frequency of 10 Hz.

As the stress distribution along the embedded length is not uniform is usual to define an average bond stress as reported in Eq.(1),

$$\tau_{\max} = \frac{F_{P_{SE772*},\max}}{\pi \times \varnothing \times (l - s)} \tag{1}$$

where: $F_{P\_SE772*,max}$ is the pull-out force (N), ϕ is the rebar diameter (mm), l is the embedded length (mm) and s is the slip between the steel bar and the SE772 * (mm).

For monotonic loading conditions, the bond stress can be calculated according to the predictive models as a function of the relative displacement as reported in Eq. (2),

$$\tau = \begin{cases} \tau_{\max}\left(\frac{s}{s_1}\right)^{\alpha} & 0 \le s \le s_1 \\ \tau_{\max} & s_1 < s \le s_2 \\ \tau_{\max} - (\tau_{\max} - \tau_f)\left(\frac{s - s_2}{s_3 - s_2}\right) & s_2 < s \le s_3 \\ \tau_f & s > s_3 \end{cases} \tag{2}$$

where the required parameters are listed in Table 2. It should be noted that these values are valid for: (i) a "good" bond condition, (ii) splitting failure, (iii) ribbed bars in which the tensile strain is lower than its yield limit. Regarding the CEB-FIP MC2010 model, the $\tau_{\max}$ value takes into account the confinement effect provided both by the concrete and the stirrups as reported in Eq. (3),

$$\tau_{u,split} = 7 \times \left(\frac{f_{cm}}{20}\right)^{0.25} \tag{3}$$

where f_{cm} is the mean cylinder compressive strength evaluated as 83% of the cubic one (MPa).

2.5. Four point loading bending test

2.5.1. Experimental setup

The beams were supported on a roller and a spin support, with a span length equal to 3810 mm (labeled hereafter "L"). A load frame was assembled and equipped with two 300 kN servo-hydraulic actuators intended to apply two pointwise loads to the beam in accordance with the four-point loading bending test setup, see Fig. 6(a).

The load was applied by a deflection rate of 2 mm/min [27–30]. A displacement sensor was connected to the piston that was loaded with "P_2" (see Fig. 6(a)) to define the correct testing speed. The pistons were connected to the same oil circuit, ensuring uniform force values

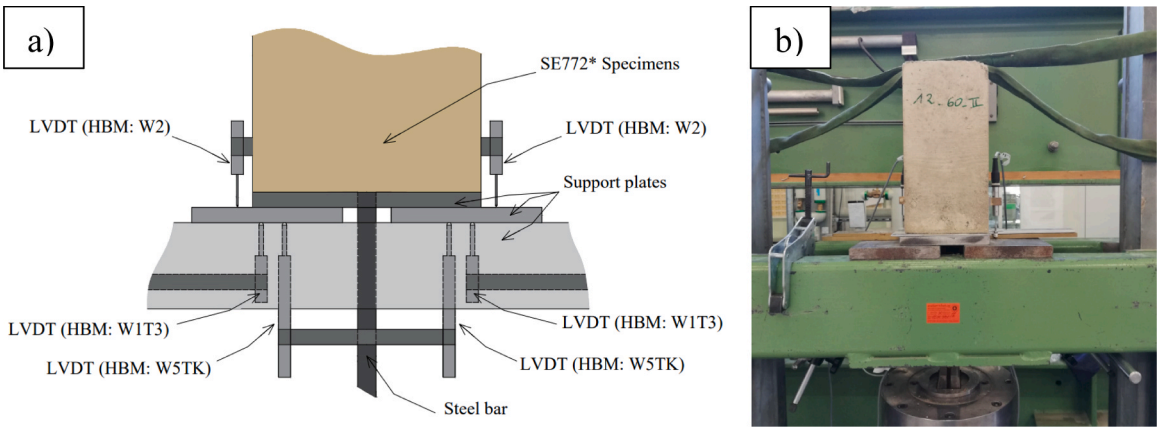

Fig. 5. a) Detail of LVDTs arrangement setup, b) Pull-out experimental setup.

Table 2
Parameters involved in the bond stress-slip relationship.

	CEB-FIP MC90	CEB-FIP MC2010
s_1	0.6 mm	$s(\tau_{u,split})$
s_2	0.6 mm	s_1
s_3	1.0 mm	1.2 s_1
α	0.4	0.4
τ_{max}	$2\sqrt{fcm}$	$\tau_{u,split}$ (Eq.(3))
τ_f	0.15 τ_{max}	0

throughout the test. A monitoring was conducted during the test to verify compliance, as both pistons were connected to force sensors. Notably, the maximum difference recorded at the point of failure, with regard to the force measured on the two pistons was less than 0.9%.

The four-point loading bending test was conducted in two distinct loading phases. The first loading step (S1) includes 3 cycles of loading-unloading performed in the elastic regime of the beam. For all 3 cycles, the minimum (P_{min}) and maximum (P_{max}) load values are 8–10 kN and 30–40 kN, respectively. S1 is requested to first simulate the mechanical response under operational loads and second to validate the loading and the support setup. In the following, the total load (P) acting on the beams is considered as the sum of two equal forces effectively applied to the beams (P_1 and P_2), see Fig. 6(a). The second loading step (S2) begins as soon as the first one is finished. S2 permits to characterize the mechanical response of the beam by applying a total load starting from P_{min} which gradually increases until to reach the total failure. As showed in Fig. 6(b), a LVDT system is fixed on the skin of the beam to measure the stretch and the midspan deflection. Specifically, four LVDTs are utilized, with two allocated to each side of the beam: one placed horizontally on the top fiber and one on the bottom fiber. An additional four LVDTs are positioned vertically on the beam: one on the extrados, one in the middle of each side, and one on the intrados fibers. Data from these LVDTs are continuously recorded using a digital acquisition system at a frequency of 10 Hz.

2.5.2. Modeling

To establish the relationship between moment and midspan deflection, a suitable model for RC is proposed in this study. The stress-strain relationships considered here involve the classical parabolic-rectangular curve with an ultimate compressive strain of 3‰ [32] for the SE. The adoption of a constitutive model typically used for concrete is supported by analyses of the mechanical properties of SE conducted in [5]. Further details regarding the stress-deformation behavior under compression are reported in [9].

Meanwhile, for the B500B steel, an elastic-plastic relationship is used, which accounts for strain hardening up to 5% of the ultimate strain. As the curvature, denoted as χ, increases, the corresponding moment, denoted as M_a, is evaluated up to the point of failure. Failure is determined either when the SE undergoes compression or when the steel bars experience traction failure. The foundational assumptions guiding this process include: (i) plane cross sections remaining plane even after deformation, and (ii) perfect adhesion between the steel reinforcement and SE, a finding supported by results presented in Section 3.2. To calibrate the model, reference was made to the mechanical properties outlined in [5].

Through the function that best approximates the χ-M_a relationship (see Fig. 7), it is possible to determine the moment of inertia J of the cross section as a function of M_a, as reported in Eq. (4),

$$J = \frac{M_a}{EM_{SE} \times \chi(M_a)} \tag{4}$$

where M_a is the bending moment (Nmm), EM_{SE} is the SE772 elastic modulus (MPa) and $\chi(M_a)$ is the curvature at a specific value of M_a (mm^{-}

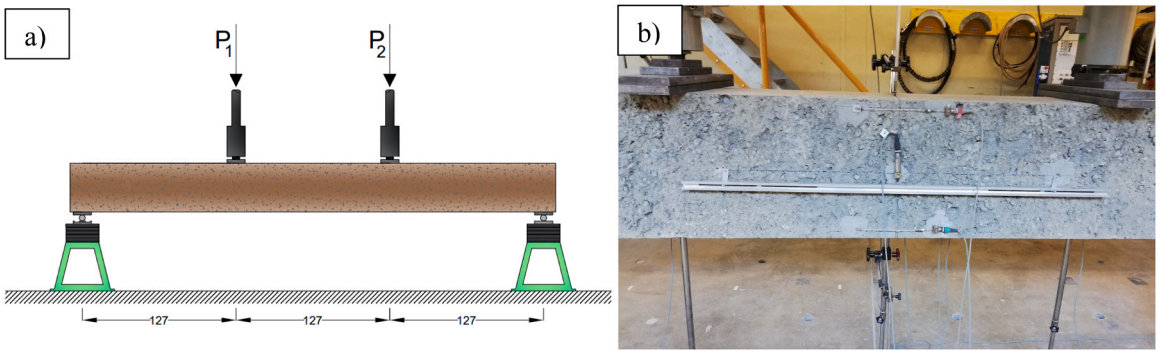

Fig. 6. a) Load pattern for four-point loading bending test b) LVDT's arrangement.